Available online at www.sciencedirect.com
SCIENCE DIRECT®
International Journal of Thermal Sciences 45 (2006) 257–268
International Journal of Thermal Sciences
www.elsevier.com/locate/ijts

Bubble and boundary layer behaviour in subcooled flow boiling

Reinhold Maurus *, Thomas Sattelmayer [1]

Lehrstuhl für Thermodynamik, Technische Universität München, 85747 Garching, Germany

Received 12 January 2004; received in revised form 7 May 2004; accepted 7 May 2004

Available online 6 October 2005

Abstract

Subcooled flow boiling is a commonly applied technique for achieving efficient heat transfer. In the study, an experimental investigation in the nucleate boiling regime was performed for water circulating in a closed loop at atmospheric pressure. The horizontal orientated test-section consists of a rectangular channel with a one side heated copper strip and good optical access. Various optical observation techniques were applied to study the bubble behaviour and the characteristics of the fluid phase. The bubble behaviour was recorded by the high-speed cinematography and by a digital high resolution camera. Automated image processing and analysis algorithms developed by the authors were applied for a wide range of mass flow rates and heat fluxes in order to extract characteristic length and time scales of the bubbly layer during the boiling process. Using this methodology, the bubbles were automatically analysed and the bubble size, bubble lifetime, waiting time between two cycles were evaluated. Due to the huge number of observed bubbles a statistical analysis was performed and distribution functions were derived. Using a two-dimensional cross-correlation algorithm, the averaged axial phase boundary velocity profile could be extracted. In addition, the fluid phase velocity profile was characterised by means of the particle image velocimetry (PIV) for the single phase flow as well as under subcooled flow boiling conditions. The results indicate that the bubbles increase the flow resistance. The impact on the flow exceeds by far the bubbly region and it depends on the magnitude of the boiling activity. Finally, the ratio of the averaged phase boundary velocity and of the averaged fluid velocity was evaluated for the bubbly region.

Keywords: Subcooled flow boiling; Bubble behaviour; Optical measurement techniques; Automated high speed video analysis; Distribution functions; Boundary layer; Velocity profile; Phase boundary velocity

1. Introduction

It is widely known, that nucleate boiling is a very efficient heat transfer mechanism and therefore plays a major role in many technical applications. Traditional examples are steam generation in fossil and nuclear power plants or the cooling of rocket engines. Besides these established fields also new applications appear at the horizon like two phase car engine cooling or the cooling of electronic devices, which serve as the technical motivation for further research on boiling in the future. Subcooled boiling is characterised by the presence of small bubbles, which grow and collapse very rapidly on or near the heated surface. These bubbles are responsible for an extremely high heat transfer augmentation. Although a huge number of publications on the topic of boiling heat transfer exist, the basic knowledge of the physical mechanisms governing the boiling process is still incomplete. Many boiling models have been derived on a semi-empirical basis or highly simplified representation of the real processes. After all, several aspects of the physics of boiling are contradictorily discussed and a full consensus has not been reached yet.

In the past, many investigations of the bubble behaviour and dynamics were performed. Due to the short time scale process, the bubble dynamics can only be resolved by high-speed cinematography with frame rates above 1000 frames per second. The pioneering work of Gunther [1] is well known. He was the first, who studied the bubble behaviour during subcooled flow boiling using the high-speed photography. He quantified successfully the bubble size, the lifetime, the growth rate and other parameters as functions of system parameters like pressure, subcooling and velocity. Also Abdelmessih et al. [2], Bibeau

* Corresponding author. Tel.: +49 89 289 16227; fax: +49 89 289 16218.
E-mail addresses: reinhold@maurus.de (R. Maurus), sattelmayer@td.mw.tum.de (T. Sattelmayer).
[1] Tel.: +49 89 28916227; fax: +49 89 28916218.

1290-0729/$ – see front matter
doi:10.1016/j.ijthermalsci.2004.05.006

Nomenclature

C	constant		
d_B	bubble diameter	m	
$\delta(L)$	boundary layer thickness	m	
F_A	cumulative distribution function		
G	liquid mass flux	$\mathrm{kg\cdot m^{-2}\cdot s^{-1}}$	
Nu	Nusselt number		
Nu_x	local Nusselt number		
L	distance from channel entrance	m	
ξ	distance from heater entrance	m	
Pr	Prandtl number		
Pos	camera position (1, 2, or 3)		
q	heat flux	$\mathrm{MW\cdot m^{-2}}$	
Re_L	Reynolds number		
Re_x	local Reynolds number		
T_{Sub}	rate of subcooling	K	
T_{Sat}	saturation temperature	K	
T_W	heater surface temperature	K	
ΔT_W	temperature difference of wall and fluid	K	
t_B	bubble lifetime	s	
$t_{B,\mathrm{Abl}}$	bubble lifetime after lift-off	s	
t_W	waiting time	s	
T	time	s	
u	local fluid velocity	$\mathrm{m\cdot s^{-1}}$	
u_0	bulk velocity	$\mathrm{m\cdot s^{-1}}$	
u^+	dimensionless fluid velocity	$\mathrm{m\cdot s^{-1}}$	
v	local velocity in normal direction	$\mathrm{m\cdot s^{-1}}$	
W_B	probability	%	
$\overline{w}_{\mathrm{PVB}}$	phase boundary velocity	$\mathrm{m\cdot s^{-1}}$	
X	coordinate streamwise	m	
Y	coordinate transverse	m	
y^+	dimensionless wall distance		

[3], Kandlikar et al. [4], Klausner et al. [5], Prodanovic [6] and others studied the bubble behaviour with optical high-speed techniques under subcooled flow boiling conditions. Due to the lack of automated evaluation methods these researchers had to analyse the recorded films manually. Single bubbles were selected and tracked in the subsequent images of the high-speed film.[2] It is obvious that due to this laborious analysis technique the results of the bubble behaviour were mostly calculated from a very limited set of bubbles and experimental conditions. Despite the low width of the database, attempts were made to derive the behaviour of the "representative" bubble from the small fraction of information on the films exploited. An additional problem for the development of a common understanding of the boiling process is that some of the effects observed in different studies are not fully consistent. Different geometrical designs of the experimental setup and the properties of the individual test fluids are a major reason for these contradictory results. For example, the orientation of the heater surface with respect to gravitation (horizontal or vertical) has a strong influence on the bubble detachment process, making a direct comparison very difficult.

The motivation for the present investigation was that a full statistical analysis of the bubble behaviour and detailed measurements of the interaction between the liquid and the vapour phase were missing. Fortunately, the quick progress digital high-speed video techniques have made in recent years and the high speed of modern computers in general allow the application of automated procedures for image processing in the future. The main standard parameters characterising the bubble behaviour are the bubble size, the lifetime, the waiting time between two cycles and the bubble density on the heater surface. While in the first part of the paper these interesting results are shortly summarised,[3] in the second part new results are presented, which describe the characteristics of the liquid phase under adiabatic and boiling conditions measured with PIV. In two phase flows most optical measurement techniques are difficult to apply without huge errors. Furthermore, the dimensionality of the problem grows due to the additional parameters of the second phase and makes a full characterisation difficult. In the past, flows with adiabatic bubbles have been investigated more often by other authors compared to flows with boiling. Marie et al. [7], for example, intensively studied the impact of adiabatic gas bubbles in vertical bubble columns. In contrast, a characterisation of subcooled boiling flows was to date exclusively performed by Hasan [8]. He investigated the velocity and temperature profile as well as the fluctuations in the bubbly region of a vertical annulus (the test fluid was the refrigerant R113) using a hot wire anemometer and the LDA technique.

2. Experimental setup

For the investigation of the bubble behaviour a test facility for flow boiling over a flat plate was built. The experimental facility was designed for water at low system pressure and the investigation of partially and fully developed subcooled flow boiling. Fig. 1 shows a sketch of the test facility. For a detailed description of the setup see Maurus et al. [9].

The closed loop allows the variation of the operating pressure, the inlet temperature and the flow velocity. Using a variable speed pump, the liquid velocity through the test-section can be adjusted between zero and 3 $\mathrm{m\cdot s^{-1}}$. The minimum subcooling is limited to 5 K due to cavitation in the pump. A heat exchanger extracts the heat transferred to the flow in the test section. The fluid degassing tank in the by-pass of the loop removes non-condensable solved gases (mainly air) by heat-

[2] Bibeau [3] started already in this direction by evaluating the size and the elongation of single bubbles using image processing and analysis algorithms.

[3] Some of these results and the analysis algorithms were already presented in previous publications of the authors [9,15].

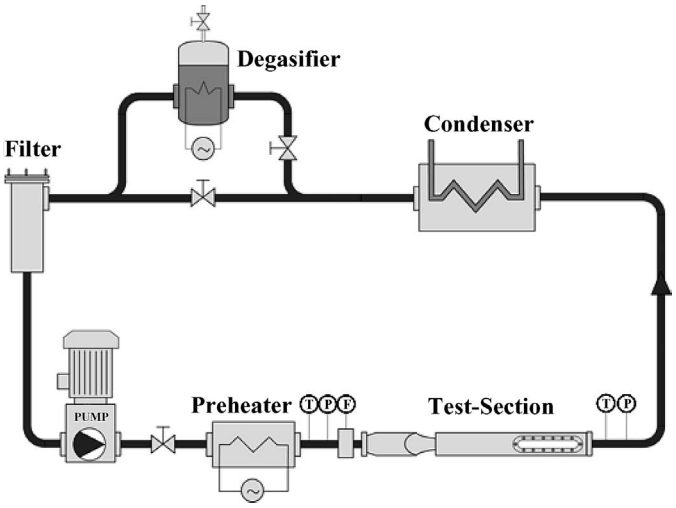

Fig. 1. Sketch of the test facility.

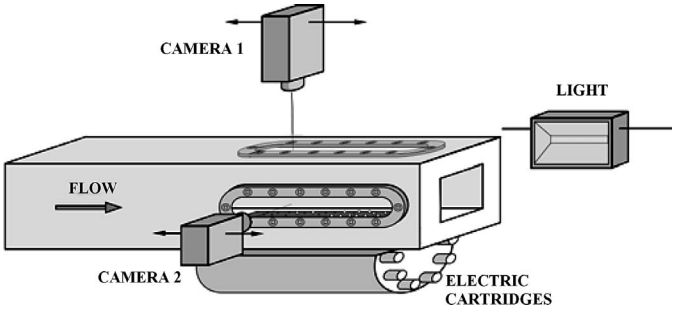

Fig. 2. Test-section and location of the cameras.

ing the fluid up to the saturation temperature. The degassing process is started hours before and continues during the experiments. All experiments were performed at steady state.

Good optical access was an important aspect for the design of the test section (see Fig. 2), which is a horizontal rectangular channel of 500 mm length with a cross-sectional area of 40 mm × 40 mm. A nozzle upstream generates uniform inflow conditions. The copper bar having a wetted surface of 15 mm width and 200 mm length is heated with electric cartridges and provides a constant heat flux boundary condition with a maximum of 1.50 $MW \cdot m^{-2}$. The heated wall section is located in the centre of the lower wall and starts 250 mm downstream of the entrance of the channel. Three observation windows allow optical access normal and parallel to the heated surface. The relatively small width of 15 mm results from a compromise between the desired two-dimensionality of the boiling process in the middle of the channel and the optical access to the central plane.

The optical arrangement is also sketched in Fig. 2. Two different cameras for the observation of the bubble behaviour are mounted on an optical bench. Camera 1 is a Sony XCD-900 with a resolution of 1280 × 960 pixels (8-bit) at a speed of 7.5 frames per second. The focal length of the receiving optics is 75 mm and the exposure time was two milliseconds. The recorded sequence is limited to seven images. Using this camera and the view perpendicular to the heated surface, the bubble density and the void fraction could be measured (see [9]). Camera 2 is a HS-Kodak Ektapro camera operated at a rate of 9000 frames per second with a resolution of 128 × 256 pixels. This speed delivers sufficient temporal resolution (0.11 ms) of the observed boiling patterns. The focal length of the receiving optics is 105 mm. For each point of operation 1000 frames were recorded. Simple backlighting was used in the high-speed video recordings. The advantage of this technique is the high light intensity, which is needed to obtain extremely short shutter times at the high frame rates employed. A tungsten lamp (500 W) and an optical diffuser plate mounted between lamp and test section generates the high intensity diffuse white light.

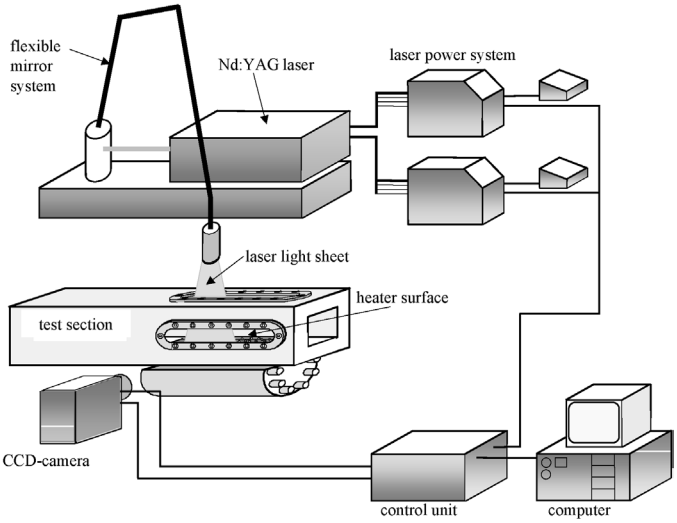

Fig. 3. Set-up of the particle image velocimeter.

Since the position of both cameras can be varied in two directions by a mechanical traverse, the boiling process can be recorded stepwise from the beginning to the end of the heater. Depending on the selected optical magnification, the accessed observation area can be varied from 10 mm up to 100 mm. Consequently, the maximum spatial resolution is about 40 micrometers per pixel for the high-speed camera and about eight micrometers for the high resolution camera. The images recorded by the high-speed camera shown subsequently cover an area of 32 mm length in main flow direction. The left side of the images is located 10 mm downstream of the beginning of the heated surface.

Using a Dantec particle image velocimeter (PIV) (e.g. [10]) the two-dimensional velocity vector map of the fluid phase could be measured. Subsequently the operation principle and the optical set-up of this technique will be briefly described. PIV provides instantaneous velocity vector measurements in a cross-section of a flow, from the pattern of the scattered light from seeding particles. The illumination is provided by two consecutive laser pulses with high energy and the light is collected by an image transfer CCD camera with high spatial resolution. The motion of the particles is evaluated by a cross-correlation algorithm.

Fig. 3 shows the components of the system used in the investigations. The test section was illuminated by two Nd:YAG

lasers, operating in the pulse mode. The wavelength of the light beam is 532 nm and each pulse has an energy of 200 mJ with a duration of 8 ns. Two criteria must be considered in selecting the optimum time delay between the two laser pulses. For high accuracy the delay should be as large as possible. However, if the upper limit given by the assumption of constant velocity between the pulses is exceeded the cross-correlation algorithm fails due to mapping problems. The typical time step used in the experiments was 100 ms. Using cylindrical lenses the laser beam was expanded to a planar light sheet with a thickness of approximately 1 mm. The scattered light from the tracer particles was recorded by the HiSense CCD camera (Hamamatsu) with a chip resolution of 1280×1024 pixels showing a display window of 24×30 mm^2. The camera was mounted on a traverse in order to provide access to the boundary layer at three different positions along the heater. These positions are identical to the positions used in the experiments with the high-speed camera. As tracer particles hollow glass spheres with a diameter of 0.01 mm and a density of 1000 kg·m^{-3} were added to the liquid. For each test parameter 100 image pairs were recorded and stored. For the calculation of the velocity vector map of each image pair the standard cross-correlation algorithm implemented in the analysis tool "FlowMap 1500" of the supplier Dantec was used. Thereby the full image was divided in 32×32 pixel sized so-called interrogation spots with an overlapping of 50%. Before a statistical analysis was performed the calculated velocity vectors had to be verified with respect to accuracy. Due to the problem of the reflection of the laser light at the phase boundaries of the bubbly layer, not all calculated vectors stem from the tracer particles. This problem could be resolved by rejecting vectors outside predefined limits for the calculated magnitude and the angle. In particular at high nucleate boiling activity this procedure leads to a rejection of up to 80% of the calculated velocity vectors in the bubbly region. After this filtering nearly all of the accepted vectors belong to the motion of the tracer particles in the liquid phase. This was validated by visual control of some velocity maps with the originally recorded image pairs. From these tests it can be concluded that the PIV measurements deliver a good measure for the average velocity distribution both in the outer region of the boundary layer and in the bubble region. For a statistical analysis of the fluid behaviour along the boundary layer an algorithm was developed, which converts the planar information of all velocity maps to a representative velocity profile by spatial and temporal averaging.

3. Algorithms for automated bubble analysis

Although many algorithms for the image quality enhancement exist, no adequate tools for the evaluation of image sequences from boiling experiments were available. For this reason, own algorithms were developed in the framework of the boiling study on the basis of MATLAB® with its image processing toolbox. Using this object orientated programming tool the effort required for the algorithm development was reduced to an acceptable level. All subsequent mentioned algorithms for the processing and analysis of single images as well as for image sequences are a combination of elements of the image processing toolbox and additional code written by the authors.

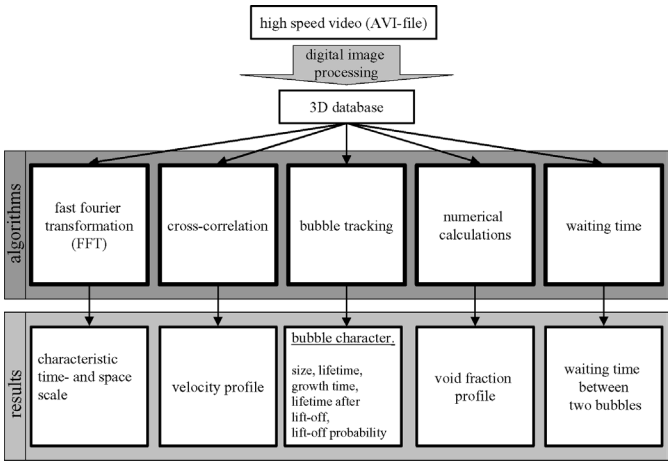

Fig. 4. Algorithms and their results.

Fig. 5. Typical image of the high-speed video film.

3.1. Image pre-processing and analysis

The processing and the analysis routine for the images of the high resolution camera (Camera 1 in Fig. 2) were already described in detail in [9]. Using the top view on the boiling surface, various boiling parameters such as the bubble density on the heater surface, the bubble size distribution, the bubble spacing as well as the void fraction were evaluated.

In order to receive temporal information concerning the bubble behaviour various high speed films at different test conditions were recorded. For the evaluation of this huge database five different algorithms have been developed and implemented in the framework of the presented study (Fig. 4). Before these algorithms were applied, a number of image pre-processing steps were needed in order to enhance the quality of all raw images (example in Fig. 5). As sketched in Fig. 6, the pre-processed images (X–Y plane) are then stacked in their temporal sequence (T-axis), generating a three-dimensional array,[4] which delivers the database for the application of the five algorithms mentioned above.

Subsequently, the 2D cross-correlation algorithm for the extraction of the phase boundary velocity profile is briefly described.

[4] The X-axis is here defined as the coordinate in downstream flow direction, the Y-axis as the coordinate normal to the flow direction. The T-axis results from the time period of the recorded high speed film.

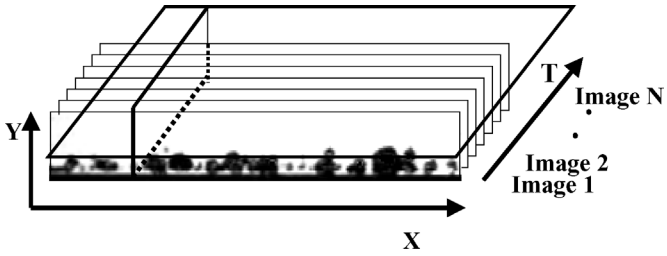

Fig. 6. Three-dimensional X–Y–T matrix.

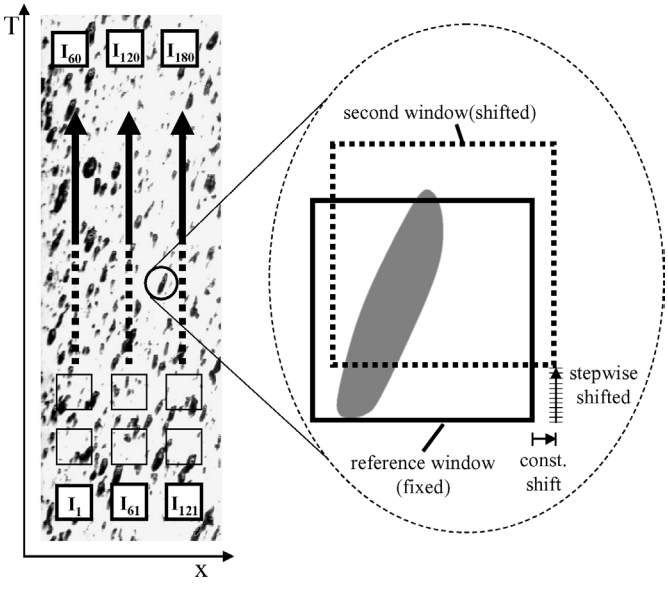

Fig. 7. Principle of the 2D cross-correlation algorithm.

3.2. Two-dimensional cross-correlation algorithm

Cross-correlation of images is useful for extracting structural similarity between two datasets. It is used in PIV in order to obtain the average particle shift between the double exposed images. While here the particles are very small and appear in form of single spots on the camera chip, the characteristic length scale is much bigger, if the velocity of the phase boundaries in the bubbly layer is of interest, like in the current study. Some similarities with the work of Smith and Dutton [11] exist, who developed a 2D cross-correlation algorithm for the determination of large scale turbulent structures. They performed a parametric study to optimise the image time delay and the correlation window size. In contrast, the information of the entire high-speed film is used in our boiling study.

Fig. 7 illustrates the developed algorithm. On the left, an image representing a part of the 3D data matrix is given. The x-, t-slice for a fixed height y above the heated surface shows the temporal movement of the bubble in the x-direction, which produces a diagonal streak in the x-, t-plane. The faster the bubble, the smaller is the angle between the streak and the x-axis. The aim of the algorithm is to find the average slope of these streaks. For this purpose, two smaller sized windows or boxes are placed in the image, as shown in Fig. 7. One box is at a fixed position while the second is shifted in x as well as in t-direction. In the first step the second box is moved with a predetermined step in

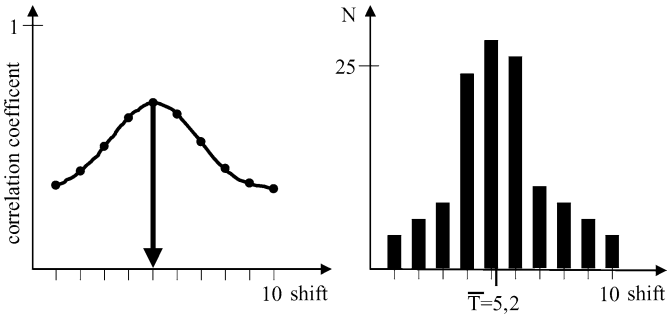

Fig. 8. Calculated correlation coefficient (left) and velocity histogram (right).

streamwise direction and afterwards it is shifted stepwise upwards passing the diagonal given by the bubble streak. At each position the fixed and the moved boxes are compared by calculating the correlation coefficient.[5] For a fixed position, the calculated correlation coefficient behaves as sketched in Fig. 8. The best similarity results in a clearly visible maximum of the correlation coefficient. After the shifting procedure has been completed, the position of the maximum of the correlation coefficient gives the bubble velocity, after the frame count at the maximum was multiplied with the shift in x-direction.

An appropriate choice of the x-shift must consider two constraints. If it is too small, the angular resolution of the streak pattern will be low. Thus, the accuracy of the deduced velocity will suffer. If the shift is too large, the similarity of the patterns of the fixed and the moving box is partially lost and no clear correlation is found. In addition, the selection of the size of the boxes must also follow certain rules. They must be large enough to capture the characteristic pattern of a streak and yet small enough to minimise the computational effort. By performing a parameter study, it was found that the optimum box contains 40×40 pixels (see Maurus and Sattelmayer [12]).

In order to obtain one representative velocity profile of the bubbly layer the x-, t-plane is divided into 180 starting positions (see I_1 to I_{180} in Fig. 7) and the mentioned procedure is applied for each position. Because not at all 180 positions the streaks are clearly visible, some criteria are defined to validate the computed coefficients. If the maximum correlation value is below a threshold or if it is not found inside the interval but instead on the boundaries, the datapoint is discarded. Otherwise it is added to the histogram in Fig. 8 in order to get the average time step, which provides together with the constant x-shift the final information of the bubble interface velocity at the given y-position.

After the computing has been completed for all y-positions of the database, an additional criterion is used to define the range, where the velocity profile can be determined with sufficient precision. For each distance from the heater (y-position) the number of valid correlations is controlled. Only if more than 80 of the 180 correlations are valid, the calculated value is se-

[5] The sum of the products between the pixel data of the fixed and the shifted box is calculated, which provides a measure of similarity. The correlation coefficient is computed, which ranges from 0 for completely dissimilar to 1 for identical datasets.

lected for the final result. As seen in Figs. 16 and 17, this is usually the case for wall distances of $0.5 < y < 1.5$ mm.

It is noted, that this procedure can be extended with the intention to measure the velocity component normal to the flow too. Here the second box has to be placed, instead on the same y-height, on a higher level above. The calculated velocity vector contains now both components, the normal and the parallel vector. This method was also applied to analyse the 3D database. Due to the small resolution of the high-speed camera the additional shift into the y-direction was only 2 pixels in order not to loose the growing bubble for the cross-correlation calculation. Consequently the uncertainty of the obtained results was very large and hence not suitable for publication.

4. Results

4.1. Flow boiling curves

In Fig. 9 various convective boiling curves for water at a constant rate of subcooling and pressure for different mass fluxes are shown. As expected, the onset of boiling depends on the fluid velocity and a velocity increase enlarges the effect of forced convection on the heat transfer. The decrease of the surface temperature for a given heat flux delays the onset of boiling. In the nucleate boiling region the heat flux rate depends strongly on the velocity, whereas in the fully developed boiling region the boiling curves merge. For high superheat, the heat transfer is dominated by the boiling process and the velocity dependence vanishes.

McAdams et al. [13] studied the subcooled flow boiling of water in a vertical annular pipe and published the following correlation:

$$q = C(T_W - T_{\mathrm{Sat}})^n \tag{1}$$

As shown in correlation 1, the heat flux depends exponentially on the wall superheat. The calculation with the given coefficients of McAdams ($n = 3.86$ und $C = 3.77$ W·m^{-2}·K^{-1}) agrees well with the experimental data in the fully developed boiling region. The exponents reported by other authors vary between 3 and 4. The value of C reported by McAdams depends mainly on the content of gas solved in the fluid. To compare the results for the lower part of the boiling curve the heat transfer for single phase over a flat plate was calculated using correlation 2 [14] for two mass fluxes ($G = 1000$ und 2000 kg·m^{-2}·s^{-1}), which are additionally displayed in Fig. 9. Here it had to be considered, that the starting point of the turbulent boundary layer development differs from the beginning of the heated surface. This can be incorporated by correcting the local Nusselt number by means of correlation 3 [14]. Both curves show, that the correlation models the measured heat transfer at the onset of nucleate boiling very well. This is a clear indication that the low width heater employed behaves similar to a fully heated wall.

$$Nu_x = 0.0308 Re_x^{4/5} Pr^{1/3} \tag{2}$$

$$Nu_x = \frac{Nu_{x(\xi=0)}}{[1-(\xi/x)^{9/10}]^{1/9}} \tag{3}$$

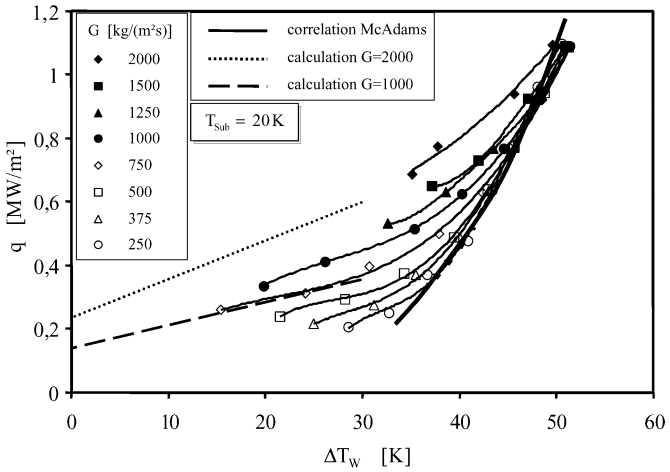

Fig. 9. Flow boiling curves.

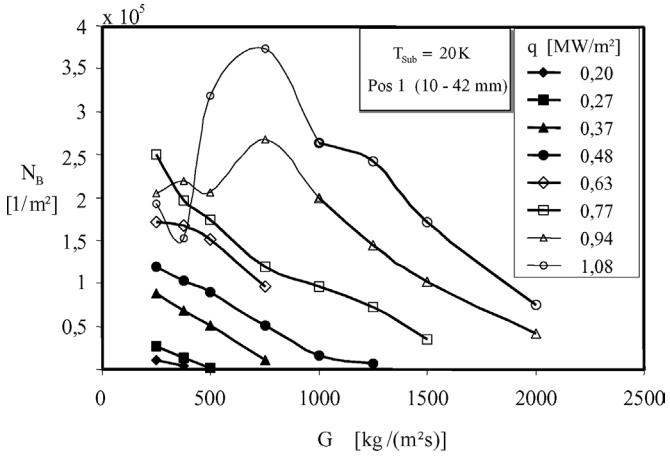

Fig. 10. Influence of the heat and mass flux on the bubble density.

The maximum heat input delivered from the cartridge heater did not allow approaching the critical heat flux of water. Fig. 9 shows clearly that in the tests the boiling patterns were observed from the onset of nucleate boiling up to the fully developed boiling regime.

4.2. Bubble characteristic

Although experimental investigations on boiling were focussed in the past on the characteristics of the "representative" bubble, the bubbles produced in nucleate boiling do not show a unique behaviour. As the analysis of the data acquired in the current study revealed an extreme wide scatter of e.g. bubble size, subsequent results are presented in form of cumulative distribution functions F_a (Figs. 11–14). The extreme width of the measured distribution indicates that averaging leads to a severe loss of information and to the wrong physical model of a fully deterministic boiling process.

4.2.1. Bubble density

Fig. 10 shows the effect of the heat flux and the liquid mass flux on the bubble density above the heater at a constant rate of subcooling and system pressure. The expression "bubble densi-

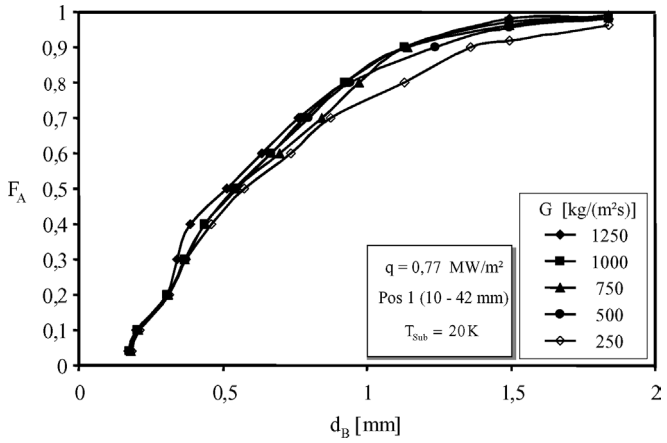

Fig. 11. Influence of the liquid mass flux on the bubble size distribution.

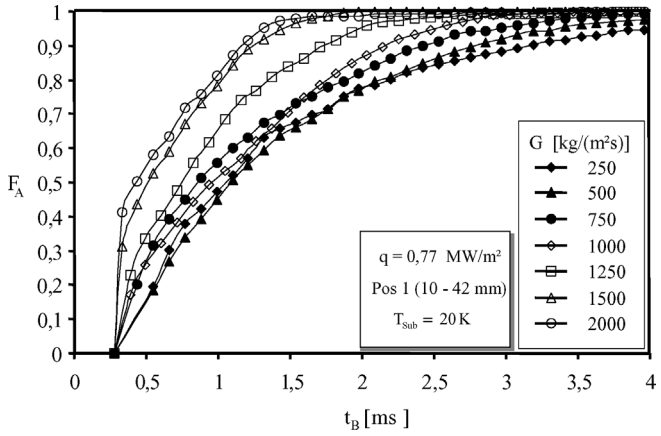

Fig. 12. Influence of the liquid mass flux on the bubble lifetime.

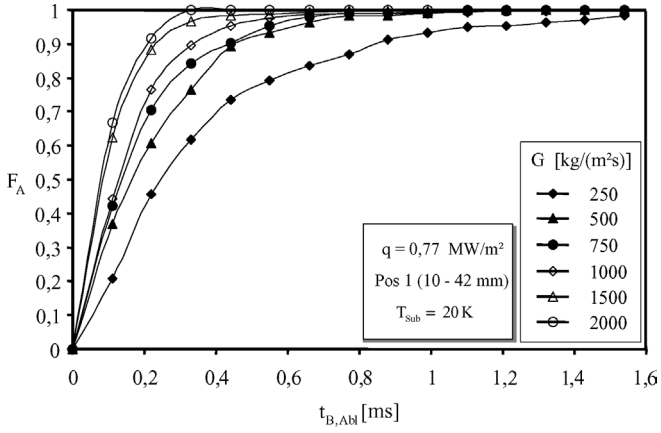

Fig. 13. Influence of the liquid mass flux on the lifetime after the bubble lift-off.

ty" represents here the average number of bubbles, which are instantly visible in the observed region of the heater. It hence differs to the idiom "nucleation side density", which summarises all nucleation sides activated during a certain period of time. These results were obtained with the vertically mounted high resolution camera. In general, increasing the heat flux leads to an increase of the bubble population. With increasing mass flux the bubble density is reduced drastically. For heat fluxes below $q = 0.77\ \mathrm{MW{\cdot}m^{-2}}$, a linear decrease is observed. Note that the curves have a very similar slope. The reason for this behaviour is the increase of the convective heat transfer with the mass flux, which leads to a decrease of the surface temperature and consequently to less activated nucleation sites. For heat fluxes above $q = 0.94\ \mathrm{MW{\cdot}m^{-2}}$, the bubbles coalesce and the number of bubbles decreases in particular for small mass fluxes. In this region (see curves with thin lines) the bubble activity becomes so strong that the limit of the measurement technique is reached.

4.2.2. Bubble size distribution

The images from the high resolution camera also contain the information about the bubble size. From these images one histogram of the bubble size for each test parameter was calculated. After integration the cumulative distribution functions shown in Fig. 11 were obtained. This figure reveals the influence of the heat flux and the convective mass flux on the size distribution.

The bubble size distribution indicates that many small bubbles are present. Fifty percent of the observed bubbles have diameters smaller than 0.5 mm. Although the bubble density depends clearly on the liquid mass flux [9], the bubble size distribution is only a very weak function of the main flow velocity. An increase of the mass flow by a factor of five decreases the bubble size only moderately.

4.2.3. Bubble lifetime

The temporal information of the bubble behaviour is evaluated by means of the bubble tracking algorithm introduced by the authors in [15]. Fig. 12 shows the effect of the mass flux on the total bubble lifetime, which includes the time difference between the nucleation process and the complete condensation and which does not take the lift-off behaviour of the bubbles into account. The distribution functions have a shape remarkably similar to the bubble size distributions (see Fig. 11). Interestingly, the data evaluation reveals clearly, that the very short lifetime of a high number of small bubbles is the physical reason behind this finding, which is consistent with the work of Bibeau [3], who also detected a strong correlation of the bubble lifetime with the bubble size. With increasing mass flux the bubble lifetime decreases and it can be seen, that for high mass fluxes ($G > 1500\ \mathrm{kg{\cdot}m^{-2}{\cdot}s^{-1}}$) no bubbles reach a lifetime of more than 1.5 ms. The results of the liquid mass flux variation show good agreement with the findings of other authors like Gunther [1], Akiyama and Tachibana [24] or Zeitoun and Shoukri [25], who also studied the bubble lifetime during subcooled flow boiling. The reason for the smaller size distribution at higher convective mass fluxes is the reduced temperature in the thermal boundary layer and the augmentation of turbulence in the cross flow. Both phenomena force the condensation at the bubble tip and limit the bubble size and lifetime.

4.2.4. Bubble lifetime after lift-off

Fig. 13 depicts the remaining lifetime of the bubbles after the lift-off from the heater surface. Similarly to the total lifetime the effect of the convective liquid mass flux is very dominant. Note that the remaining lifetime is roughly one order of magnitude smaller than the total lifetime. The strong influence of the mass

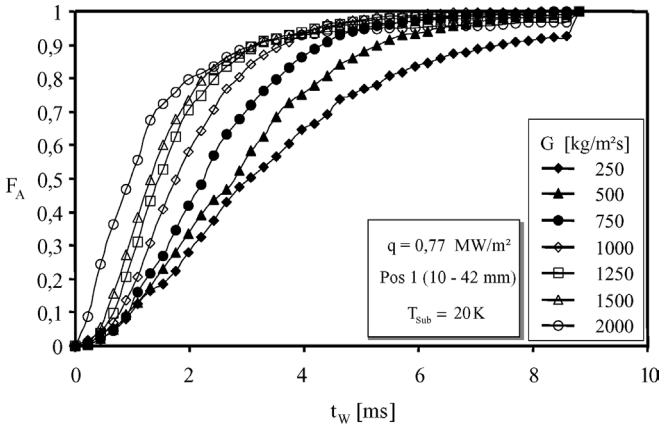

Fig. 14. Influence of the liquid mass flux on the waiting time between two bubble cycles.

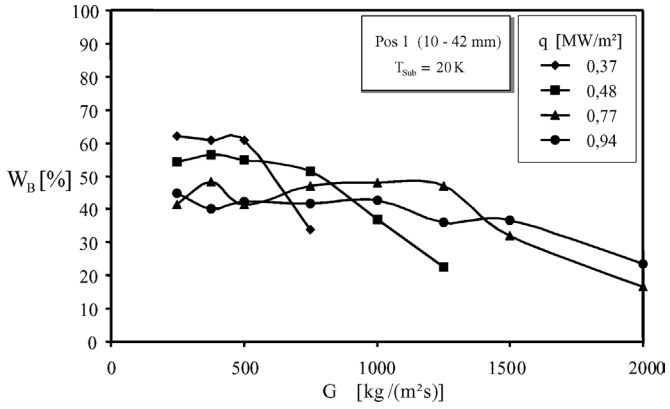

Fig. 15. Influence of the liquid mass flux and the heat flux on the bubble lift-off probability.

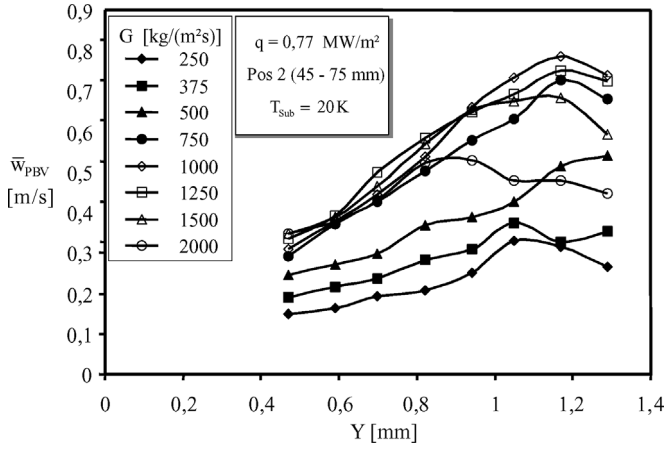

Fig. 16. Effect of the liquid mass flux on the phase boundary velocity profile.

flux can be explained again by the increasing slip between both phases and the augmentation of turbulence in the liquid. The latent heat of the condensing vapour, which heats up the liquid near the bubble interface, is more effectively convected into the bulk liquid leading to a larger the temperature difference and condensation rate. This effect explains also the negligible influence of the heat fluxes at constant mass flux. Similar findings were described earlier by Lucic et al. [16], who studied the heat transfer around single condensing bubbles in vertical subcooled flow boiling with holographic interferometry.

4.2.5. Waiting time between two bubble cycles

The waiting time between two bubble cycles was also detected, using the fifth algorithm shown in Fig. 4. Fig. 14 shows the effect of the liquid mass flux on this parameter. With increasing mass flux the waiting time is significantly reduced and shows the trend already found for the bubble lifetime. Interestingly, the waiting time is only very weakly influenced by the heat flux. Only a slight reduction is observed with increasing heat flux.[6]

4.2.6. Lift-off probability

In addition to the results concerning the time scales of the boiling process, information about the detachment behaviour were extracted from the database. Fig. 15 shows the lift-off probability, which is indicated with the parameter W_B on the vertical axis, of the analysed bubbles for different mass- and heat fluxes. For all parameters the probability W_B lies between 20 and 65 percent. For small mass fluxes ($250 < G < 500$ kg·m^{-2}·s^{-1}) the fraction of bubbles, detaching from the surface, is independent of the mass flux. An increase the mass flux above this range leads to a drop of the lift-off probability. Whether bubbles detach from the surface or not was contrarily discussed in the past. Del Valle and Kenning [17] observed no bubble lift-off for horizontal subcooled flow boiling. In contrast, Bibeau [3] and Thorncroft [18] described that almost all studied bubbles detach during vertical subcooled flow boiling. These bubbles were carried away in streamwise direction until they condensed far away from their nucleation site. Obviously, the orientation of the gravitational field is crucial. The liquid drag and buoyancy are perpendicular for horizontal heater surfaces. In case of a vertical heater orientation both forces act in the same direction and foster the bubble detachment.

4.2.7. Phase boundary velocity profile (PBV)

Using the two-dimensional cross-correlation algorithm, the axial phase boundary velocity profile for different mass fluxes at constant values of subcooling and heat flux was determined (see Fig. 16). For all mass fluxes the velocity increases with increasing distance from the heater (from 0.5 mm to 1 mm). The PBV is very sensitive to the mass flux below $G < 750$ kg·m^{-2}·s^{-1}. In contrast, the influence vanishes for higher values. At bigger distances from the heater surface, the effect of bubble collapse plays an important role for the development of the PBV profile. This leads to a velocity decrease. In Fig. 17 the influence of different heat fluxes on the PBV profile is shown. For distances up to one millimeter, the PBV shows no dependence on the heat flux. For higher distances the bubble growth and the bubble collapse affect the measured PBV considerably. In [12], the influence of the subcooling on the PBV was additionally published. With increasing rates of subcool-

[6] See figure in [15]. In this paper, the results are discussed and compared with the findings of other authors.

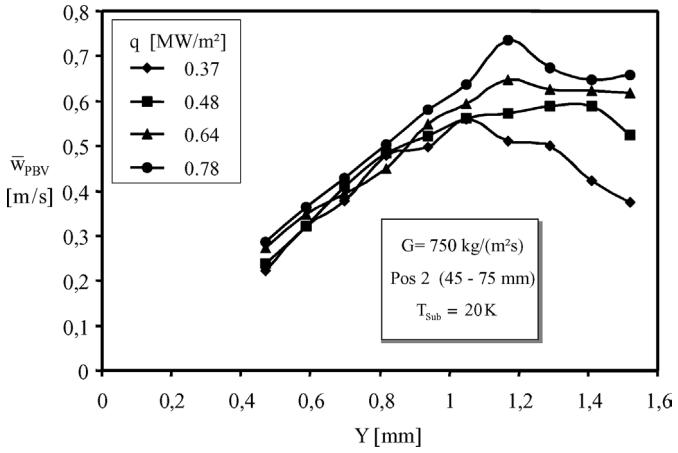

Fig. 17. Influence of the heat flux on the phase boundary velocity profile.

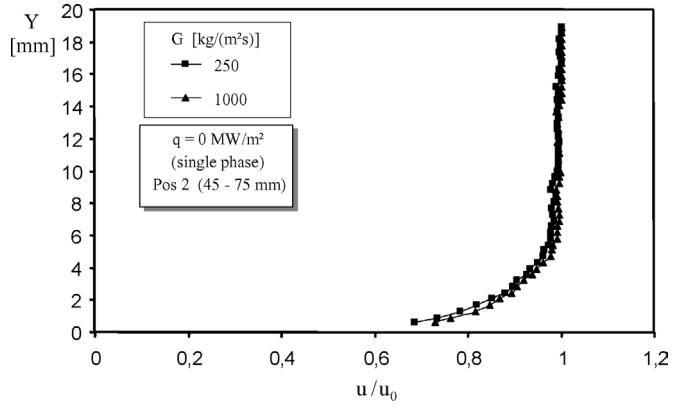

Fig. 18. Normalised velocity profile for single phase flow.

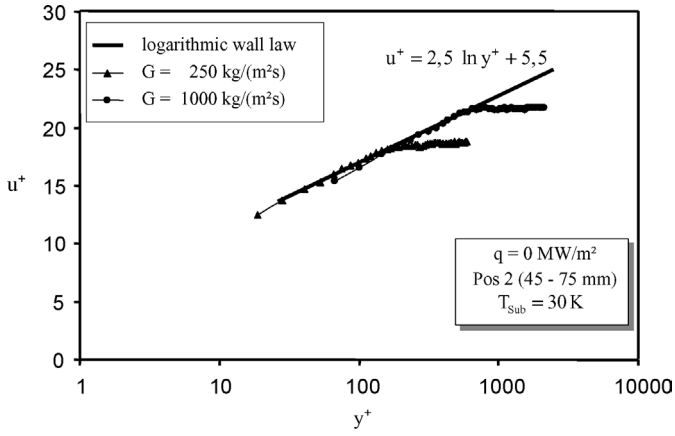

Fig. 19. Semi-logarithmic velocity profile plot.

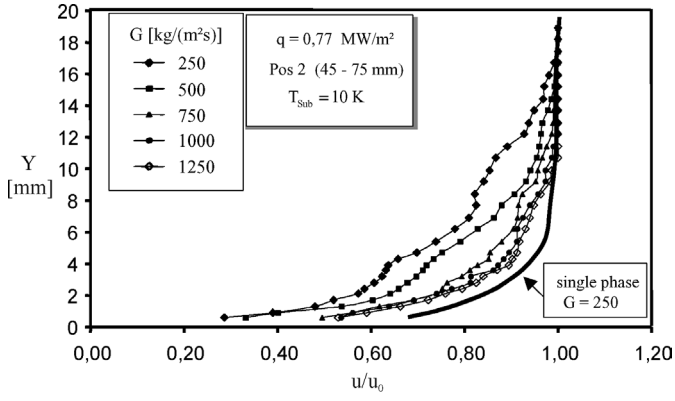

Fig. 20. Influence of the liquid mass flux on the axial velocity component.

ing, the PBV profile decreases, while the slope of the profile curves increases. The height, where the bubble collapse mainly takes place, is shifted to smaller values.

4.3. Characteristics of the boundary layer

4.3.1. Velocity profiles

PIV measurements were first performed in single phase flow for the mass fluxes 250 and 1000 $\mathrm{kg{\cdot}m^{-2}{\cdot}s^{-1}}$, which serve as reference data for the velocity distribution in the liquid phase of subcooled boiling flow. Fig. 18 shows the velocity profiles over the heater surface, whereby both mass fluxes were normalised to the bulk flow velocity. The strong velocity decrease towards the surface in the boundary layer becomes clearly visible. The thickness of the boundary layer is approximately 7 mm. Eq. (4) [19] predicts 7.6 mm for the mass flux of $G = 1000\ \mathrm{kg{\cdot}m^{-2}{\cdot}s^{-1}}$ and a boundary layer length of 0.3 m. The single phase measurements were performed at a fluid temperature of 70 °C in order to keep liquid viscosity as close as possible to the two-phase flow investigated in the next step.

$$\delta(L) = 0.381(Re_L)^{-0.2}L \tag{4}$$

In order to check, whether the velocities in the boundary layer follow the logarithmic wall law for turbulent flow, the measurements were plotted in the semi-logarithmic form $u^+ = f(y^+)$. For the determination of the shear stress it is assumed, that the wall law is partially valid and the data is fitted in this region to the logarithmic profile. The result of this procedure agrees well with the prediction of the wall law of Prandtl for tube flows [20]. The results also correspond well with the findings of Kang et al. [21], who studied the isothermal and heated turbulent upflow in a vertical annular channel. After the calculation of the shear stress, the profiles $u^+ = f(y^+)$ in Fig. 19 are obtained, which indicate that the flow over the heater closely follows the law for turbulent boundary layers, although the Reynolds number in the heated channel is around 10^5–10^6 and hence probably still weakly turbulent.

4.3.2. Velocity profile of the liquid phase with nucleate boiling

Fig. 20 shows the time averaged velocity profiles in flow direction for different mass fluxes and in addition the velocity profile of the single phase flow for comparison. All velocity profiles are normalised with the related mean bulk velocity. The vapour bubbles influence the velocity distribution in the bubbly region as well as in the layer above, where no bubbles exist. This becomes particularly visible for the lowest investigated mass flux of $G = 250\ \mathrm{kg{\cdot}m^{-2}{\cdot}s^{-1}}$. Although the thickness of the bubbly layer is restricted to the zone of approximately 6 mm over the heater, the impact of the bubbles on the averaged velocity profile of the forced flow is clearly visible almost up to the middle of the channel 20 mm above the heater. It can be seen,

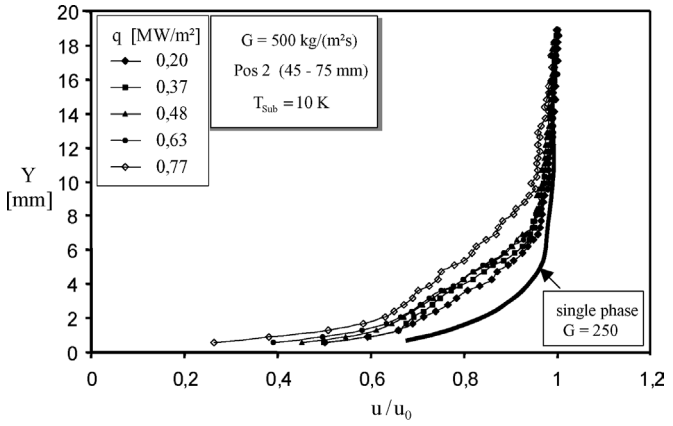

Fig. 21. Influence of the heat flux on the axial velocity component.

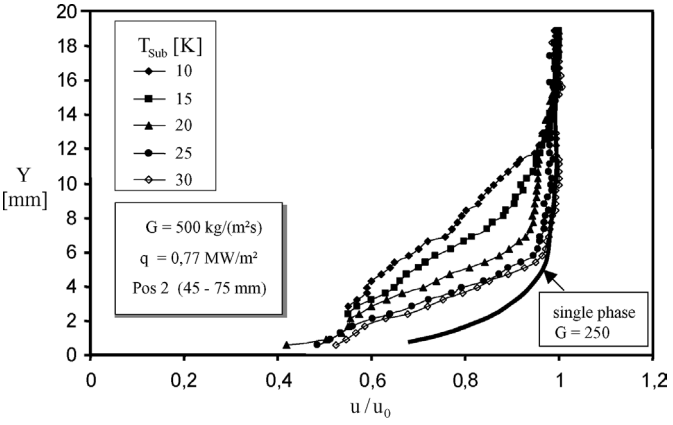

Fig. 22. Influence of the rate of subcooling on the axial velocity component.

that for all mass fluxes the bubbles lead to a decrease of the velocity and hence to an additional pressure drop. This effect, which was postulated earlier by various authors (e.g., [22,23]), is quantitatively shown for the first time in this investigation. Fig. 21 depicts the influence of the heat flux on the axial velocity profile for a constant mass flux of $G = 500\ \mathrm{kg{\cdot}m^{-2}{\cdot}s^{-1}}$. By increasing the heat flux the boiling process is augmented and hence the velocity in flow direction decreases. In order to compare the two phase profile with the single phase flow, the reference velocity profile[7] for $G = 250\ \mathrm{kg{\cdot}m^{-2}{\cdot}s^{-1}}$ is additionally plotted in Fig. 21. The effect of subcooling is shown in Fig. 22. Going towards to the saturation temperature the bubble size and hence the impact on the profile increases.

The PIV measurement also delivers information of the velocity component normal to the flow. While this velocity is very small in single phase flow, it increases considerably during boiling. Due to the bubble growth the fluid above the bubble head is accelerated from the boundary layer towards the centre of the channel. The effect of the mass flux on the normal velocity component is shown in Fig. 23 and the influence of the heat flux in Fig. 24. It can be seen, that the maximum velocity is reached at a distance of approximately 1 mm above the heater. With increasing distance to the wall the velocity decreases. For low mass fluxes of $G = 250\ \mathrm{kg{\cdot}m^{-2}{\cdot}s^{-1}}$ the normal velocity reaches remarkably high values of around 60% of the bulk velocity and the bubbles influence the flow almost to the channel centre. With increasing mass flux or decreasing subcooling the thickness of the impact zone as well as the velocity ratio decreases (see Figs. 24 and 25). Specially for $T_{\mathrm{Sub}} = 10$ K and for heat fluxes higher than $q = 77\ \mathrm{MW{\cdot}m^{-2}}$ the normal velocity component is huge, due to the achievement of the netto–vapour–production point (see [3]), where the condensation process is reduced by the small thermal gradient

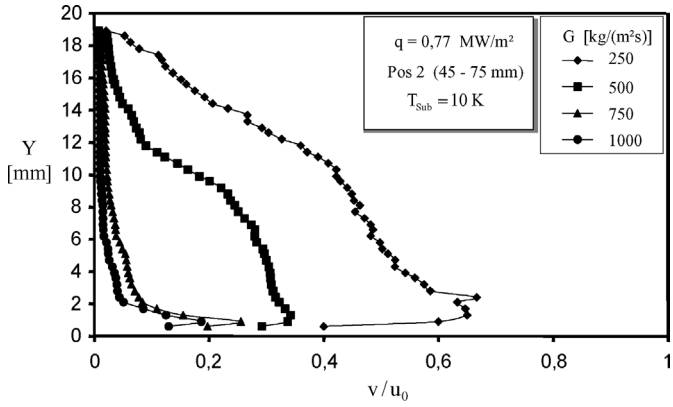

Fig. 23. Influence of the liquid mass flux on the normal velocity component.

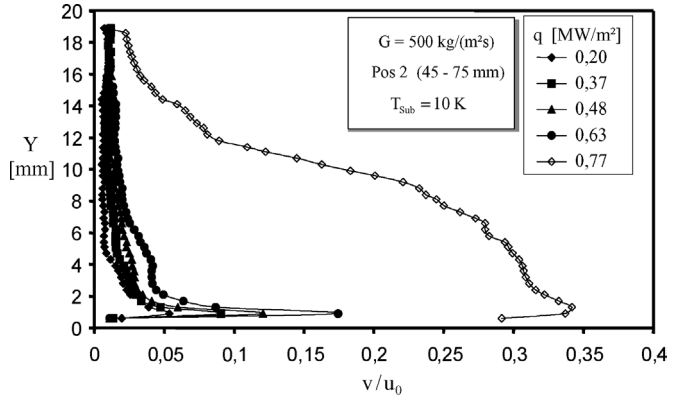

Fig. 24. Influence of the heat flux on the normal velocity component.

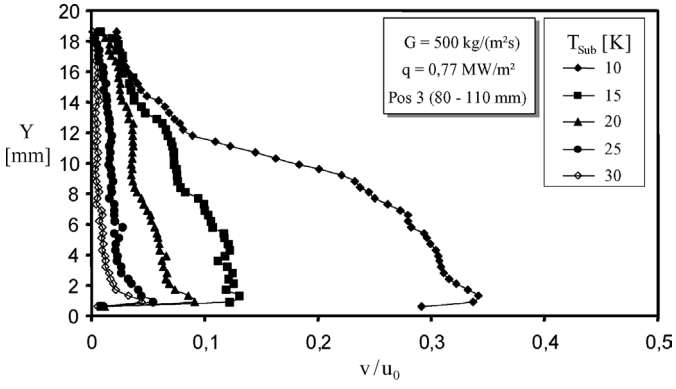

Fig. 25. Influence of the rate of subcooling on the normal velocity component.

[7] The corresponding single phase velocity profile $G = 500\ \mathrm{kg{\cdot}m^{-2}{\cdot}s^{-1}}$ was not investigated. In regard to the results in Fig. 18 it can be assumed, that the present normalised velocity profile would not differ significantly.

between the liquid and the vapour phase. This leads to an accelerated bubble growth and hence to an enlargement of the void fraction, which also limits the application of this measurement technique. Since for all investigated mass fluxes the average normal velocity was approximately 0.15 to 0.20 $m \cdot s^{-1}$, it can be concluded that the fluid motion normal to the main flow direction is almost independent of the mass flux of the cross flow. As already mentioned only the results of Hasan [8] are available for comparison. He investigated the velocity profile with the LDA in the bubbly region of a vertical annular flow of refrigerant R113. The results agree qualitative with the findings of the current study. Full quantitative agreement is not obtained due to the differing properties of water and refrigerant R113.

4.3.3. Comparison of the liquid and the phase boundary velocities

The velocities of the single phase and the velocities of the phase boundary in the bubbly region are now compared for different test parameters. For this purpose, the axial phase boundary velocities, which are calculated by the cross-correlation algorithm described previously, and the axial fluid velocity from the PIV measurements are now averaged for four fixed distances above the heater ($Y = 0.5$, $Y = 0.85$, $Y = 1.2$ and $Y = 1.5$ mm). The investigated range cannot be extended further, because at bigger distances from the heater no bubbles exist for high mass fluxes or low heat fluxes. The ratio of the averaged phase boundary velocity and the averaged fluid velocity is plotted over four different test parameters as shown in Fig. 26. In each case one parameter is varied while the others are kept constant. These reference values are defined in the legend of Fig. 26.

For small heat fluxes, high rates of subcooling and for high heat fluxes the averaged phase boundary velocity is smaller than the averaged axial fluid velocity. For all other test parameters an opposite trend is visible. In particular for small mass fluxes of $G = 250$ $kg \cdot m^{-2} \cdot s^{-1}$ the velocity ratio plotted at the y-coordinate reaches nearly 2. With increasing mass flux the velocity ratio decreases approximately linear. The degree of subcooling shows a similar trend. The phase boundary moves quicker when the heat flux is increased.

In addition, a remarkable increase of the PBV along the length of the heater in streamwise direction becomes visible, if the measurements taken at the three different positions are compared. The reason for this increase is the development of the thermal boundary layer, which leads to an increase of the liquid temperature in the bubbly layer and to an augmentation of the bubble growth.

Interestingly, all effects shown in Fig. 26 correlate qualitatively with the average bubble size. This finding is caused by two different effects. The first one is the influence of the bubbles on the flow. Small bubbles generate only moderate flow resistance and flow deceleration, whereas bigger bubbles have a higher impact on the flow velocity (Fig. 20). The second effect appears in cases with bigger bubbles. While small bubbles are due to the strong surface tension almost spherical, the shape of bigger bubbles changes significantly during their lifetime. Due to the drag forces of the cross flow, which increase from the

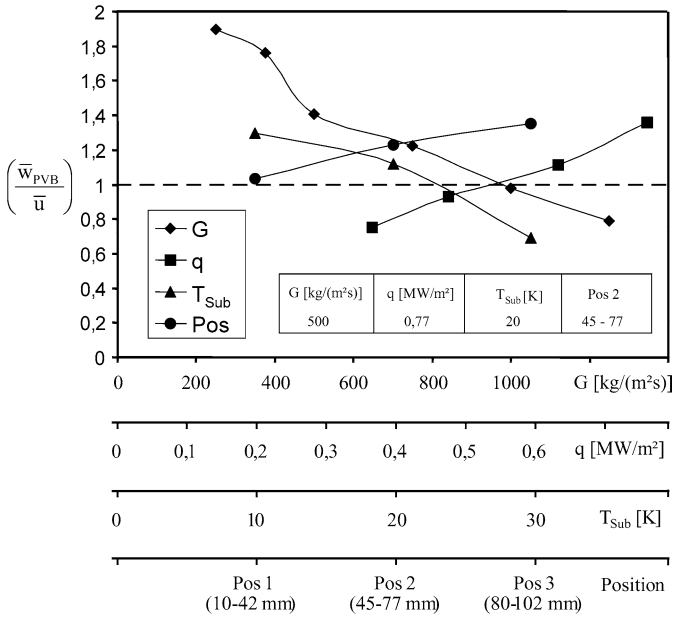

Fig. 26. Ration of the averaged phase boundary velocity profile and the averaged fluid velocity profile in the bubbly region.

wall towards the bulk flow, the bubble contour is stretched into main flow direction. This results in an increased phase boundary velocity.

Gunther [1] as well as Akiyama and Tachibana [24] observed that the bubble velocity is smaller than the fluid velocity. Their tests were performed at high mass fluxes and at high rates of subcooling. At small heat fluxes an opposite trend was noted by Bibeau [3] and by Thorncroft [18]. Both findings agree qualitatively well with the findings displayed in Fig. 26.

4.4. Uncertainty analysis

Experimental errors for quantities measured directly were obtained from manufacturer's specifications. Errors associated with calculated parameters were estimated using error propagation methods. Due to the use of calibrated thermocouples the uncertainty for the heater surface temperature is around ± 0.8 K. The error for the heat flux prediction is ± 0.05 $MW \cdot m^{-2}$ and around ± 25 $kg \cdot m^{-2} \cdot s^{-1}$ for the liquid mass flux. The uncertainty of bubble parameters is based on two reasons. Firstly, the temporal and spatial resolution of the high speed camera is limited. In the present case the time resolution, which depends on the selected frame rate, is 0.11 ms and the spatial resolution is around 0.13 mm. The uncertainty becomes especially for small bubbles with short lifetime more evident. The second reason for the uncertainty is the functionality of the developed algorithms for the automated bubble analysis, which had to be investigated. This was performed by comparing the automated results with some manually analysed film sequences. It was ascertained, that for all comparisons both results agreed well within the range of $\pm 10\%$. The uncertainty for the PIV results are similarly based one two effects. The first one mentions the well-known systematical and statistical error of this measurement technique for the velocity vector calculation due to optical aberration, tim-

ing error and the use of the cross-correlation algorithm for the displacement of the seeding particles [10]. Because of the high resolution of the PIV camera and the moderate velocities of the tracer particles (compared to other fields of investigations), the following second effect is estimated to be much more dominant. PIV measurement in two phase flow is difficult because of the previously mentioned laser light reflection at the bubble phase boundaries. This unavoidably leads to a number of spurious vectors, which have to be removed by various settings (see Chapter 2). Anyway, it cannot be ascertained that all these vectors calculated from light reflection are successfully removed. Due to the spatial and temporal averaging of 100 image pairs the total error of the axial and normal velocity components is estimated to $\pm 5\%$ of the bulk velocity u_0.

5. Conclusions

In the present study boiling experiments in subcooled flow under atmospheric pressure conditions were conducted. The boiling process was visualised with two different optical measurement techniques. Using digital image processing and analysis algorithms developed by the authors an automated evaluation of the high-speed films was performed. The automated procedures allowed the evaluation of a wider database and the full quantification of the statistics of the boiling process. For the first time the bubble behaviour is presented in form of distribution functions. These reveal strong scatter of the bubble dynamics and size. In addition, the liquid velocities and the phase boundary velocities were measured. The bubbles have a clear impact on the velocity distribution in the liquid phase, which depends strongly on the strength of the boiling activity. Under boiling conditions the velocity profile is remarkably decelerated in the bubbly region. Interestingly, this effect exists also above the bubbly layer, although no bubbles are present there. The velocity normal to the flow can reach remarkable values and is highest at the bubble tip, where the fluid is pushed towards the channel centre. Finally, the fluid velocity profile in the bubbly region was compared with the boundary layer velocity. While both velocities are almost equal for test conditions with small bubbles, the phase boundary velocity exceeds the fluid velocity in cases, which are favourable for the formation of larger bubbles.

Acknowledgements

The authors highly appreciate the financial support of the Deutsche Forschungsgemeinschaft (DFG) in the frame of the joint research project on fundamentals of boiling heat transfer. Special thanks go to Norbert Krasznai for his engaged help on performing the PIV measurements and to Volodymyr Ilchenko for coding the cross-correlation algorithm.

References

[1] F.C. Gunther, Photographic study of surface-boiling heat transfer to water with forced convection, Trans. ASME 73 (1951) 115–123.

[2] A.H. Abdelmessih, F.C. Hooper, S. Nangia, Flow effects on bubble growth and collapse in surface boiling, Int. J. Heat Mass Transfer 15 (1972) 115–125.

[3] E. Bibeau, Void growth in subcooled flow boiling for circular and finned geometries for low values of pressure and velocity, PhD thesis, University of British Columbia, 1993.

[4] S. Kandlikar, V. Mizo, M. Cartwright, Investigation of bubble departure mechanism in subcooled flow boiling of water using high-speed photography, in: Convective Flow Boiling Conf., Banff, Canada, 1995.

[5] J.F. Klausner, R. Mei, M. Bernhard, L.Z. Zeng, Vapour bubble departure in forced convection boiling, Int. J. Heat Mass Transfer 36 (3) (1993) 651–662.

[6] V. Prodanovic, Bubble behaviour in subcooled flow boiling at low pressures and flow rates, PhD thesis, University of British Columbia, 2001.

[7] J.L. Marie, E. Moursali, S. Tran-Cong, Sililarity law and turbulence intensity profiles in a bubbly boundary layer at low void fractions, Int. J. Multiphase Flow 23 (1997) 227–247.

[8] A. Hasan, Turbulent subcooled boiling and nonboiling flow through a vertical concentric annular channel, PhD thesis, Arizona State University, 1991.

[9] R. Maurus, V. Ilchenko, T. Sattelmayer, Study of the bubble characteristics and the local void fraction in subcooled flow boiling using digital imaging and analysing techniques, J. Exp. Thermal Fluid Sci. 26 (2–4) (2002) 147–155.

[10] M. Raffel, C. Willert, J. Kompenhans, Partial Image Velocimetry, Springer, Berlin, 1998.

[11] K.M. Smith, J.C. Dutton, A procedure for turbulent structure convection velocity measurements using time-correlated images, Experiments Fluids 27 (1999) 244–250.

[12] R. Maurus, T. Sattelmayer, Bubble behaviour and phase boundary velocity in subcooled flow boiling using high speed cinematography and novel digital imaging analysis, in: Proc. Conf. of Thermophysical Properties and Transfer Processes of New Refrigerants, Session B5, Paderborn, 2001.

[13] W.H. McAdams, W.E. Kennel, C.S. Minden, R. Carl, P. Picornell, J.E. Dew, Heat transfer at high rates to water with surface boiling, Ind. Engrg. Chem. 41 (9) (1949) 1945–1953.

[14] F.P. Incropera, D.P. DeWitt, Fundamentals of Heat and Mass Transfer, John Wiley and Sons, New York, 1996.

[15] R. Maurus, V. Ilchenko, T. Sattelmayer, Automated high-speed video analysis of the bubble dynamics in subcooled flow boiling, J. Exp. Thermal Fluid Sci. 25 (2) (2004) 149–158.

[16] A. Lucic, M. Emans, F. Mayinger, C. Zenger, Interferometric study and numerical simulation of the temperature field in the boundary layer and heat transfer in subcooled flow boiling, in: Proc. 5th International Conference on Boiling Heat Tran., Jamaica, 2003.

[17] M.V. Del Valle, D.B. Kenning, Subcooled flow boiling at high heat flux, Int. J. Heat Mass Transfer 28 (1985) 1907–1920.

[18] G.E. Thorncroft, Heat transfer and vapor bubble dynamics in forced convection boiling, PhD thesis, University of Florida, 1997.

[19] E. Truckenbrodt, Fluiddynamik, Band 2, Auflage 4, Springer, Berlin, 1999.

[20] H. Schlichting, Grenzschicht-Theorie, Verlag G. Braun, Karlsruhe, 1982.

[21] S. Kang, B. Patil, J.A. Zarate, R.P. Roy, Isothermal and heated turbulent upflow in a vertical annular channel—Part I. Experimental measurements, Int. J. Heat Mass Transfer 44 (2001) 1171–1184.

[22] F. Mayinger, Strömung und Wärmeübergang in Gas-Flüssigkeits-Gemischen, Springer, Berlin, 1982.

[23] W.G.J. (van) Helden, On detaching bubbles in upward flow boiling, PhD thesis, TU Eindhoven, 1994.

[24] M. Akiyama, F. Tachibana, Motion of vapor bubbles in subcooled heated channel, Bull. JSME 17 (104) (1974).

[25] O. Zeitoun, M. Shoukri, Bubble behaviour and the mean diameter in subcooled flow boiling, Trans. ASME J. Heat Transfer 118 (1996) 110–116.